MOX-Report No. 13/2016

Computational study of the risk of restenosis in coronary bypasses

Guerciotti, B; Vergara, C; Ippolito, S; Quarteroni, A; Antona, C;

Scrofani, R.

MOX, Dipartimento di Matematica
Politecnico di Milano, Via Bonardi 9 - 20133 Milano (Italy)

mox-dmat@polimi.it http://mox.polimi.it

Computational study of the risk of restenosis in coronary bypasses

Bruno Guerciotti[1] Christian Vergara[1] Sonia Ippolito[2]
Alfio Quarteroni[3] Carlo Antona[4] Roberto Scrofani[4]

[1] MOX - Department of Mathematics, Politecnico di Milano, Piazza Leonardo da Vinci 32, 20133 Milano, Italy
[2] Radiology Unit, Ospedale L. Sacco, via G.B. Grassi 74, 20157 Milano, Italy
[3] SB MATHICSE CMCS, EPFL, av. Piccard, Bat. MA, Sec. B2-C2, Station 8, CH-1015 Lausanne, Switzerland
[4] Cardiosurgery Unit, Ospedale L. Sacco, via G.B. Grassi 74, 20157 Milano, Italy

Abstract

Coronary artery disease, caused by the build-up of atherosclerotic plaques in the coronary vessel wall, is one of the leading causes of death in the world. For high-risk patients, coronary artery bypass graft is the preferred treatment. Despite overall excellent patency rates, bypasses may fail due to restenosis. In this context, the purpose of this work is to perform a parametric computational study of the fluid-dynamics in patient-specific geometries with the aim of investigating a possible relationship between coronary stenosis degree and risk of graft failure. Firstly, we propose a strategy to prescribe realistic boundary conditions in absence of measured data, based on an extension of Murray's law to provide the flow division at bifurcations in case of stenotic vessels and non-Newtonian blood rheology. Then, we carry out numerical simulations in three patients affected by severe coronary stenosis and treated with a graft, in which the stenosis degree is virtually varied in order to compare the resulting fluid-dynamics in terms of hemodynamic indices potentially involved in restenosis development. Our findings suggest that low degrees of coronary stenosis produce a more disturbed fluid-dynamics in the graft, resulting in hemodynamic conditions that may promote a higher risk of graft failure.

Keywords: coronary bypass; restenosis; Murray's law; non-Newtonian rheology; computational fluid-dynamics

1 Introduction

Coronary artery disease (CAD) is one of the leading causes of death in the world, accounting for 7.2 million deaths/year, which equates to 12% of all deaths worldwide [3]. CAD is caused by the build-up of atherosclerotic plaques in the coronary vessel wall, resulting in a reduction of oxygen supply to the heart and possibly leading to cardiovascular-related events such as myocardial infarction, stroke and unstable angina.

Depending on the characteristics of the atherosclerotic lesions (e.g. severity, number and site), several alternative treatments exist for CAD, including medical therapy, endarterectomy, balloon angioplasty, stenting and coronary artery bypass graft (CABG) surgery. For high-risk patients, such as those with left main coronary artery (LMCA) disease and severe ventricular dysfunction, CABG is the preferred treatment [16, 38]. In particular, the "gold standard" procedure for the surgical treatment of left anterior descending (LAD) coronary artery disease is the left internal mammary artery (LIMA) bypass, because of its excellent long-term patency of nearly 90% at 15 years [49]. This is due to the physiological properties of LIMA, which is able to retain its intrinsic properties in the endothelium and smooth muscle cells and to adapt and autoregulate in response to changes in blood flow demand and hemodynamic conditions [45].

Despite overall excellent patency rates, increasing frequency of restenosis of the LIMA grafts has been noted, particularly in the region of the anastomosis between LIMA and LAD [2, 46]. Different hypotheses have been formulated to explain a possible correlation between hemodynamics and restenosis at the LIMA anastomosis. Among them, the presence of recirculating flows, characterized by low and oscillatory wall shear stress (WSS), is thought to be the main cause of intimal lipid accumulation with consequent macrophages recruitment and inflammation, which eventually lead to plaque formation [2, 13, 17, 46]. In fact, hemodynamic patterns at CABG anastomoses exhibit flow separation, recirculation and stagnation zones [47, 55] and several clinical studies have reported the evidence that competitive flow (i.e. a relatively high flow through LAD, compared to LIMA), arising in patients with less-than-critical stenosis of the recipient artery, may cause particularly disturbed flow at the anastomotic site with subsequent graft failure [4, 29, 31]. This evidence suggests that the long-term patency of LIMA may be intrinsically related to the degree of stenosis in the native vessel and, in particular, it may be promoted by the presence of non-severe stenoses. Although the possible failure of LIMA graft nowadays represents a clinical evidence, some controversy still exists about the pertinence of LIMA bypasses in case of moderate grades of stenosis [39].

Computational methods have been effectively employed to investigate quantitatively and non-invasively the fluid-dynamics in coronary artery bypass grafts in idealized models [17, 23, 42, 47, 55], in animal geometries [26], and, more recently, in human geometries [19, 41, 53]. Very few studies [10, 32, 48, 55] have examined the possible relationship between competitive flow and risk of LIMA restenosis at the anastomotic region. In this context, the purpose of this study is to investigate, by means of computational tools, the interplay between the severity of LAD stenosis and the risk of restenosis of LIMA bypass in patient-specific geometries.

To this aim, the first goal of this work is to propose, within this context, a possible solution to prescribe realistic boundary conditions in absence of measured data. In particular, in order to estimate the flow division between LMCA and LAD, which is expected to be a function of the stenosis degree, we propose an extension of the well known Murray's law, originally proposed in Murray [30] for non-stenotic vessels and Newtonian fluids, to the case of stenotic vessels and non-Newtonian fluids. The resulting flow division is a function of the physical properties of the branching vessels, i.e. dimensions, blood viscosity, degree of stenosis.

The second aim of this work is to provide a computational study of the fluid-

dynamics in three patients affected by LAD stenosis and treated with a LIMA graft. In particular, we perform a parametric study based on Finite Element Analysis and on the proposed extension of Murray's law, in patient-specific geometries reconstructed from CT images in which the degree of the stenosis is virtually varied from 40% to 90%. We investigate a possible relationship between LAD stenosis and risk of graft failure in terms of well-known WSS-based hemodynamic indices potentially involved in plaque formation and restenosis development.

2 Materials and Methods

2.1 Patients recruitment

For this study, we consider three patients (P1, P2 and P3 in what follows) with isolated severe LAD disease (i.e. stenosis greater than 70%) who underwent off-pump CABG surgery with LIMA to LAD bypass graft. Myocardial revascularization was achieved by standard stabilization with Octopus device and by use of intracoronary shunt.

A Philips Brilliance CT 64-slice system was employed to perform a follow-up study based on three-dimensional Contrast Enhanced Computed Tomography (3D-CE-CT). The main parameters of the acquisition are: slice thickness $0.67mm$, slice spacing $0.33mm$, reconstruction matrix 512×512 pixels, final resolution $0.45mm \times 0.45mm \times 0.33mm$.

2.2 Computational domains and mesh generation

By using a level-set segmentation technique developed in the software VMTK (http://www.vmtk.org), we reconstructed a surface model of the interface between the blood and the arterial wall from the CT images of the three patients, thus defining the 3D computational domain. In particular, we reconstructed the LMCA with its two main branches, the LAD and the left circumflex artery (LCx), and the LIMA graft (see Figure 1, right). For each patient we also created the following further 3D computational domains:

- a domain without stenosis and bypass in order to simulate the "healthy" case (*healthy* domain, see Figure 1, left, for an example, case P1);
- six *diseased* domains with different degrees of LAD stenosis, from 40% to 90% (see Figure 1, middle, for an example with a stenosis of 70%, case P1).
- six *surgically-treated* domains with different degrees of LAD stenosis featuring a LIMA bypass (see Figure 1, right, for an example with a stenosis of 70%, case P1);

To create these virtual geometries, we developed ad-hoc scripts in VMTK which allowed us to virtually remove the stenosis and the bypass, and to change the degree of stenosis, maintaining the same original eccentricity.

Then, the computational domains were turned into volumetric meshes of tetrahedra in view of the numerical simulations. In particular, the computational meshes were obtained after a refinement study with the aim of achieving

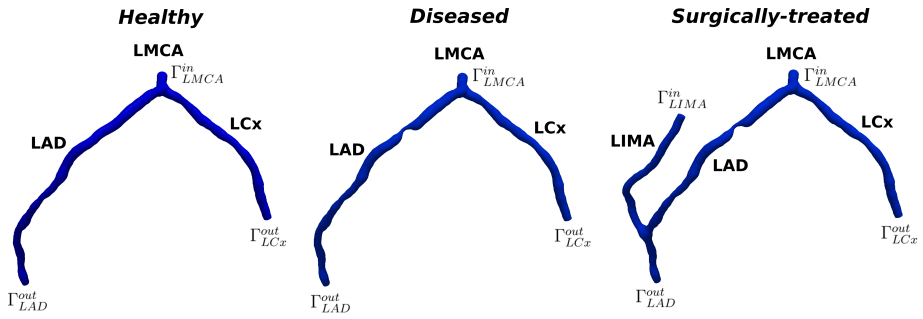

Figure 1: Computational domains for the numerical simulations (patient P1). Left: *healthy* geometry. Middle: *diseased* geometry (i.e. without LIMA bypass). Right: *surgically-treated* geometry (i.e. with LIMA bypass)

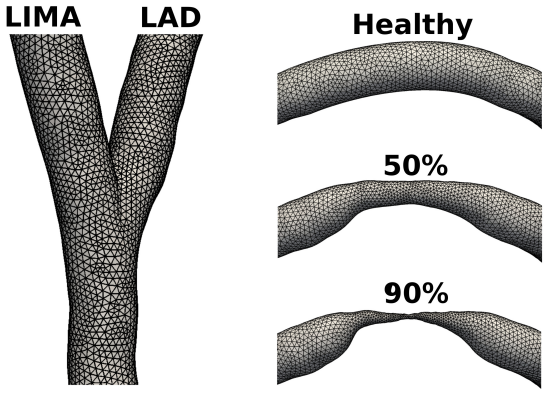

Figure 2: Mesh details for patient P3. Left: anastomosis between LIMA and LAD. Right: different degrees of LAD stenosis

mesh-independent numerical solutions on the velocity and WSS up to a tolerance of 2%. A local mesh refinement was performed at the level of the LAD stenosis, proportional to the degree of the stenosis. The resulting number of tetrahedra of the *surgically-treated* domains were about 800,000 for P1, 750,000 for P2 and 600,000 for P3. In Figure 2, we report an example of the meshes of P3 regarding the LIMA-LAD anastomosis and the LAD stenosis.

2.3 Extension of Murray's law to stenotic vessels and non-Newtonian rheology

To impose suitable boundary conditions at the outlets of our domain, we need to quantify the flow division occurring at the LMCA bifurcation (see Figure 1). With this aim, we start by deriving an expression of the flow rate in a stenotic vessel as a function of the pressure gradient and of the physical parameters characterizing the vessel.

We represent a stenotic vessel as the sequence of three cylindrical segments V_i, $i = 1, 2, 3$, of length l_1, l_2, l_3 and radius $r_1 = r$, $r_2 = \alpha r$ and $r_3 = r$,

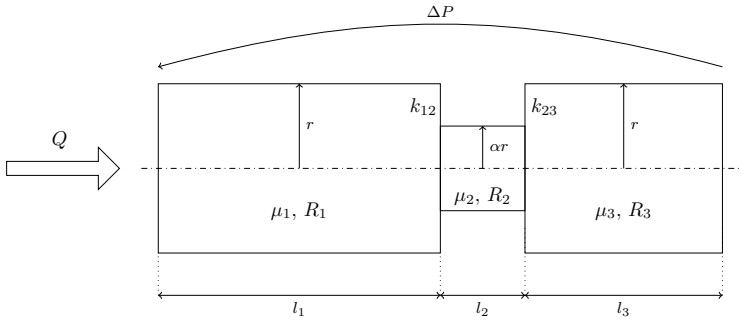

Figure 3: Schematic representation of a vessel of radius r with a stenosis of radius αr. Each vessel segment V_i, $i = 1, 2, 3$, is characterized by viscosity μ_i and resistance R_i. The additional resistance due to the changes of area are characterized by loss coefficients k_{12} and k_{23}

respectively, where α, $0 < \alpha \leq 1$, is the degree of stenosis (see Figure 3).

The total resistance of the vessel is given by the sum of the resistances R_i of each segment (regarded as isolated segments) plus two terms which account for the additional pressure drops, say F_{12} and F_{23}, due to the changes of area between segments V_1 and V_2 and between V_2 and V_3. The resistances of each segment V_i are obtained under the assumption of Poiseuille flow. In particular, the volumetric flow rate Q is linearly proportional to the pressure drop ΔP_i:

$$Q = \frac{1}{R_i}\Delta P_i,$$

where the resistance R_i is defined as [7]

$$R_i = \frac{8\mu_i l_i}{\pi r_i^4}. \tag{1}$$

Notice that, since we are assuming a non-Newtonian fluid, in principle the viscosities μ_i are different in each segment. The additional pressure drops due to the change of area are given by [7]

$$F_l = \frac{w}{2}\rho k_l \bar{v}_2^2, \quad l = 12, 23,$$

where ρ is the fluid density, $\bar{v}_2$ the average fluid velocity at the stenosis V_2, and k_l, $l = 12, 23$, suitable coefficients which account for the energy related to the area restriction and expansion, respectively, and whose expression depends on the type of area variation. Notice that we multiplied the expression of the additional pressure drops by the weight

$$w = 1 - e^{\frac{\alpha-1}{\alpha}},$$

allowing one to obtain a null contribution of these terms for the case without stenosis ($\alpha = 1$).

Thus, the power W_f required to maintain the flow in the vessel is given by

$$\begin{aligned} W_f = Q\Delta P &= Q\left(\sum_{i=1}^{3}\Delta P_i + F_{12} + F_{23}\right) \\ &= \left(R_1 + R_2 + R_3\right)Q^2 + w\frac{\rho}{2}\left(k_{12}\bar{v}_2^2 + k_{23}\bar{v}_2^2\right)Q. \end{aligned} \tag{2}$$

By using the relation $Q = \bar{v}_2 A_2$, where $A_2 = \pi r_2^2 = \pi\alpha^2 r^2$ is the vessel area at the stenosis, and substituting (1) into (2), we get

$$\begin{aligned} W_f = &\frac{1}{r^4}\left[\frac{8}{\pi}\left(\mu_1 l_1 + \frac{\mu_2 l_2}{\alpha^4} + \mu_3 l_3\right)Q^2\right. \\ &\left. + \frac{w\rho}{2\pi^2\alpha^4}\left(k_{12} + k_{23}\right)Q^3\right]. \end{aligned} \tag{3}$$

Following Murray [30], we need to account for an additional power, W_m, given by the metabolic requirement, which increases linearly with the volume of blood and, for each of the cylindrical segment, is given by [43]

$$W_{m,i} = m\pi r_i^2 l_i,$$

where m is a metabolic coefficient accounting for the blood cells metabolism. Thus, in our case we have that the total metabolic power is given by

$$W_m = \sum_{i=1}^{3} W_{m,i} = m\pi r^2\left(l_1 + \alpha^2 l_2 + l_3\right). \tag{4}$$

Putting (3) and (4) together, we can evaluate the total power requirement as

$$W_{tot} = \frac{1}{r^4}\left(c_1 Q^3 + c_2 Q^2\right) + c_3 r^2, \tag{5}$$

with $c_1 = \frac{w\rho}{2\pi^2\alpha^4}\left(k_{12} + k_{23}\right)$, $c_2 = \frac{8}{\pi}\left(\mu_1 l_1 + \frac{\mu_2 l_2}{\alpha^4} + \mu_3 l_3\right)$ and $c_3 = \pi m\left(l_1 + \alpha^2 l_2 + l_3\right)$.

For given values of the coefficients c_1, c_2 and c_3 (i.e. fixing the geometry, the fluid properties and the blood metabolism characteristics) and for a specified value of Q, W_{tot} depends only on r. Thus, it makes sense to look for the value of r which minimizes W_{tot}. By imposing $dW_{tot}/dr = 0$, we obtain

$$\frac{dW_{tot}}{dr} = -\frac{4}{r^5}\left(c_1 Q^3 + c_2 Q^2\right) + 2c_3 r = 0,$$

which can be rearranged as

$$aQ^3 + bQ^2 + d = 0, \tag{6}$$

where we set $a = 4c_1$, $b = 4c_2$ and $d = -2c_3 r^6$. The solutions of the previous third-order equation are given by

$$\begin{aligned} Q &= Q^{sten}(r, \alpha, \mu_1, \mu_2, \mu_3, l_1, l_2, l_3) \\ &= \sqrt[3]{\left(-\frac{b^3}{27a^3} - \frac{d}{2a}\right) + \sqrt{\left(-\frac{b^3}{27a^3} - \frac{d}{2a}\right)^2 + \left(-\frac{b^2}{9a^2}\right)^3}} \\ &+ \sqrt[3]{\left(-\frac{b^3}{27a^3} - \frac{d}{2a}\right) - \sqrt{\left(-\frac{b^3}{27a^3} - \frac{d}{2a}\right)^2 + \left(-\frac{b^2}{9a^2}\right)^3}} \\ &- \frac{b}{3a}. \end{aligned} \tag{7}$$

This is an expression of the flow rate in a stenotic vessel of degree α which depends on the geometrical parameters of the vessel, the fluid properties and the blood metabolic characteristics.

In case there is no stenosis (i.e. $\alpha = 1$), then $c_1 = 0$ and (6) reduces to

$$bQ^2 + d = 0,$$

leading to

$$Q = \sqrt{-\frac{d}{b}} = \sqrt{\frac{c_3}{2c_2}} = \sqrt{\frac{\pi^2 m}{16\mu}} r^3. \tag{8}$$

Equations (7) and (8) can be used to estimate the flow division between a healthy parent vessel (with flow rate Q_p, radius r_p and viscosity μ_p) and a stenotic daughter vessel (with flow rate Q_d and parameters r_d, $\mu_{1,d}$, $\mu_{2,d}$,$\mu_{3,d}$, $l_{1,d}$, $l_{2,d}$, $l_{3,d}$), leading to

$$\frac{Q_d}{Q_p} = \frac{Q^{sten}(r_d, \alpha, \mu_{1,d}, \mu_{2,d}, \mu_{3,d}, l_{1,d}, l_{2,d}, l_{3,d})}{\sqrt{\frac{\pi^2 m}{16\mu_p}} r_p^3}. \tag{9}$$

In the particular case where also the daughter vessel is not stenotic, from the previous expression we obtain the following flow division

$$\frac{Q_d}{Q_p} = \sqrt{\frac{\mu_p}{\mu_d}} \left(\frac{r_d}{r_p}\right)^3, \tag{10}$$

where r_d and μ_d are the radius and the viscosity of the daughter vessel. Notice that, in case of Newtonian fluid (i.e. $\mu_p = \mu_d$), the original Murray's law,

$$\frac{Q_d}{Q_p} = \left(\frac{r_d}{r_p}\right)^3, \tag{11}$$

is recovered.

In practice, the metabolic coefficient m is needed to compute c_3 and thus d in (7). However, this value is hardly achievable from clinical measures. For this reason, we propose here to use the value of the flow rate of the parent vessel given by (8) to provide a suitable estimate of m:

$$m(t) = \frac{16\mu_p(t) Q_p(t)^2}{\pi^2 r_p^6}. \tag{12}$$

This is the value used in our numerical simulations, as Q_p was known.

2.4 Numerical simulations and boundary conditions

We consider blood as a homogeneous and incompressible fluid described by the Navier-Stokes equations [12] and we assume a non-Newtonian rheology model (see Discussion). In particular, we choose the Carreau-Yasuda model, with viscosity given by [9, 53]

$$\mu(\boldsymbol{x}, t) = \mu_\infty + (\mu_0 - \mu_\infty)\left(1 + (\lambda \dot{\gamma}(\boldsymbol{x}, t)^a\right)^{\frac{n-1}{a}}, \tag{13}$$

where $\lambda = 1.902s$, $n = 0.22$, $a = 1.25$, $\mu_0 = 0.56P$, $\mu_\infty = 0.0345P$ and the shear rate given by $\dot{\gamma} = 2\sqrt{D_{II}}$, where D_{II} denotes the second invariant of the rate of deformation tensor $\boldsymbol{D} = \frac{1}{2}\left(\nabla \boldsymbol{u} + (\nabla \boldsymbol{u})^T\right)$, with $\boldsymbol{u} = \boldsymbol{u}(\boldsymbol{x}, t)$ being the velocity of the fluid. For blood modelled as an incompressible fluid, the second invariant is $D_{II} = \frac{1}{2}\sum_{i,j=1}^{3} D_{ij}D_{ij}$. Notice that in fact the viscosity given by (13) is a function of the velocity, i.e. we can write $\mu = \mu(\boldsymbol{u})$.

We perform unsteady numerical simulations using the Finite Element library LifeV (http://www.lifev.org). The vessel walls are considered rigid. We use $P1_{bubble} - P1$ finite elements for the space discretization and the backward Euler method with a semi-implicit treatment of the convective term for the time discretization, setting the time discretization parameter $\Delta t = 0.01s$ [36]. The non-linearity arising from the non-Newtonian model (13) is treated semi-implicitly. This means that, indicating with z^n the approximation of a generic function $z(t)$ evaluated at $t^n = n\Delta t$, $n = 1, \ldots$, at each time-step t^n we have the following discretized-in-time problem to be solved in the computational domain Ω:

$$\begin{cases} \rho_f \dfrac{\boldsymbol{u}^n - \boldsymbol{u}^{n-1}}{\Delta t} - \mu(\boldsymbol{u}^{n-1})\nabla \cdot \left(\nabla \boldsymbol{u}^n + (\nabla \boldsymbol{u}^n)^T\right) \\ \quad + \rho_f \boldsymbol{u}^{n-1} \cdot \nabla \boldsymbol{u}^n + \nabla p^n = \boldsymbol{0} & \text{in } \Omega, \\ \nabla \cdot \boldsymbol{u}^n = 0 & \text{in } \Omega, \end{cases}$$

equipped with suitable initial and boundary conditions, where $\rho_f = 1.06 g/cm^3$ is the fluid density and p the fluid pressure.

Referring to Figure 1, right, that depicts one representative geometry with stenosis and bypass included in our study, we observe that we need to prescribe boundary conditions at the two inlets, Γ^{in}_{LIMA} and Γ^{in}_{LMCA}, and at the two outlets, Γ^{out}_{LAD} and Γ^{out}_{LCx}. Since neither patient-specific velocity nor pressure data are available, we select two representative flow rate waveforms $\widetilde{Q}_{LMCA}(t)$ and $\widetilde{Q}_{LIMA}(t)$ for the inlets reported in the literature for proximal LMCA and LIMA, see Keegan et al [20] and Sakuma et al [40]. We depict these waveforms in Figure 4 where the peak values are set to $1\, cm^3/s$, so that the effective flow rates prescribed are

$$Q_{LMCA}(t) = \gamma_{LMCA}\widetilde{Q}_{LMCA}(t) \tag{14}$$

and $Q^X_{LIMA}(t) = \gamma^X_{LIMA}\widetilde{Q}_{LIMA}(t)$, for suitable constants γ_{LMCA} and γ^X_{LIMA}, $X = 40, \ldots, 90$, to be determined, X representing the degree of stenosis. Notice that the flow rate at Γ^{in}_{LMCA} does not depend on X, whereas the one at Γ^{in}_{LIMA} does since the body supplies the decreased flow rate in LAD due to the stenosis by increasing the flow rate in LIMA. The value of γ_{LMCA} is set for each patient so as to adapt it to the dimensions of LMCA and to obtain physiological velocity values, see Table 1.

In order to find reasonable values of γ^X_{LIMA}, we make the following hypothesis, which is supported by several clinical and exprimental evidence [29, 33, 34]:

Hp) In presence of a LIMA bypass, assuming that the latter works properly, the blood flow rate feeding the myocardium through Γ^{out}_{LAD} remains constant regardless of the degree of LAD stenosis, i.e.

$$Q^X_{LAD}(t) + Q^X_{LIMA}(t) = K(t), \tag{15}$$

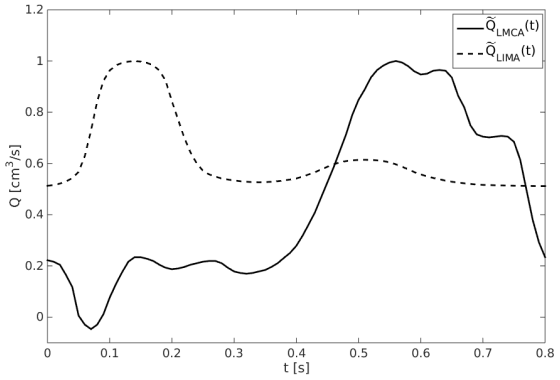

Figure 4: Representative flow rate waveforms $\widetilde{Q}_{LMCA}(t)$ and $\widetilde{Q}_{LIMA}(t)$, where the peak values were set to 1 cm^3/s

P1	P2	P3
1.021	0.692	0.769

Table 1: Values of γ_{LMCA} for each patient needed to obtain the patient-specific flow rate $Q_{LMCA}(t) = \gamma_{LMCA}\widetilde{Q}_{LMCA}(t)$ to be imposed as inflow boundary condition at Γ^{in}_{LMCA}

for a suitable function of time K that does not depend on X (Q^X_{LAD} being the flow rate flowing in LAD with degree of stenosis X). Moreover, the flow rate feeding the myocardium $K(t)$ is the same we have in absence of stenosis and bypass, i.e. in a healthy scenario.

Accordingly, we firstly solve for each patient an auxiliary problem in the corresponding *healthy* geometry, reported in Figure 1, left, in order to estimate the flow rate $Q^H_{LAD}(t)$ at Γ^{out}_{LAD} (see Auxiliary problem 1 below). This allows us to determine $K(t)$, since in this case (15) reduces to

$$Q^H_{LAD}(t) = K(t). \tag{16}$$

Then, we perform for each patient six more auxiliary numerical simulations (one for each degree of stenosis) in the *diseased* geometry reported in Figure 1, middle (see Auxiliary problems 2 below). This allows us to estimate the flow rates in the LAD for the diseased cases, $Q^X_{dis,LAD}$, $X = 40, 50, \ldots, 90$. Assuming that the flow rate at LMCA is independent of the presence of the bypass and of the degree of stenosis, from the extended Murray's law (9) we have that these flow rates are the same also in the *surgically-treated* cases ($Q^X_{dis,LAD} = Q^X_{LAD}$). Thus, owing to (15) and (16), we have that the flow rate at Γ^{in}_{LIMA} for each degree of stenosis is given by

$$Q^X_{LIMA}(t) = Q^H_{LAD}(t) - Q^X_{dis,LAD}(t). \tag{17}$$

However, we notice that the LAD flow rate is diastolic, whereas the LIMA flow rate is systolic. In order to avoid non-realistic waveforms due to this offset,

(17) is to be intended as a time-averaged relation. This allows us to compute the values of γ^X_{LIMA} for each degree of stenosis and for each patient, see Final problems below.

Summarising, for each patient we need to solve, at each discrete time t^n, the following discretized-in-time Navier-Stokes problems:

Auxiliary problem 1. *Healthy* geometry (see Figure 1, left) with the following boundary conditions:

- Flow rate condition at Γ^{in}_{LMCA}:

$$\int_{\Gamma^{in}_{LMCA}} \boldsymbol{u}^n \cdot \boldsymbol{n}\, d\gamma = Q_{LMCA}(t^n), \tag{18}$$

  where $\boldsymbol{n}$ is the outward unit normal and Q_{LMCA} is given by (14);

- Flow rate condition at Γ^{out}_{LAD}. Relation (10) can be used for the flow division between LMCA and LAD ($p = LMCA$, $d = LAD$), yielding

$$\int_{\Gamma^{out}_{LAD}} \boldsymbol{u}^n \cdot \boldsymbol{n}\, d\gamma = Q^H_{LAD}(t^n) = \sqrt{\frac{\mu^n_{LMCA}}{\mu^n_{LAD}}} \left(\frac{r_{LAD}}{r_{LMCA}}\right)^3 Q_{LMCA}(t^n),$$

  where r_{LAD} and r_{LMCA} are representative radii of LAD and LMCA districts. As an approximation of LMCA and LAD viscosities, we use a spatial average of $\mu(\boldsymbol{u}^{n-1})$ over the LMCA and LAD domains Ω_{LMCA} and Ω_{LAD}, respectively:

$$\mu^n_{LMCA} = \frac{1}{|\Omega_{LMCA}|} \int_{\Omega_{LMCA}} \mu(\boldsymbol{u}^{n-1}(\boldsymbol{x}))d\omega,$$

$$\mu^n_{LAD} = \frac{1}{|\Omega_{LAD}|} \int_{\Omega_{LAD}} \mu(\boldsymbol{u}^{n-1}(\boldsymbol{x}))d\omega.$$

- A zero-traction condition at Γ^{out}_{LCx}:

$$-p^n \boldsymbol{n} + \mu\left(\boldsymbol{u}^{n-1}\right)\left(\nabla \boldsymbol{u}^n + (\nabla \boldsymbol{u}^n)^T\right)\boldsymbol{n} = \boldsymbol{0}. \tag{19}$$

After solving the Auxiliary problem 1, we are able to compute the averaged-in-time flow rate

$$\overline{Q}^H_{LAD} = \frac{1}{N}\sum_{n=1}^{N} Q^H_{LAD}(t^n),$$

where N is the number of discrete time instants within a heartbeat.

Auxiliary problems 2. *Diseased* geometries (one for each degree of stenosis, see Figure 1, middle) with the following boundary conditions:

- Flow rate condition (18) on Γ^{in}_{LMCA};

- Flow rate condition at Γ^{out}_{LAD}:

$$\int_{\Gamma^{out}_{LAD}} \boldsymbol{u}^n \cdot \boldsymbol{n}\, d\gamma = Q^X_{dis,LAD}(t^n) \qquad X = 40, \dots, 90,$$

where $Q^X_{dis,LAD}$ is computed owing to (7).

The metabolic coefficient m in (7) is estimated by means of formula (12) with $p = LMCA$, while the loss coefficients k_{12} and k_{23}, associated with the area contraction/expansion due to the stenosis, are set equal to 0.5 and 1, respectively [7].

- Zero-traction condition (19) at Γ^{out}_{LCx}.

Owing to the Auxiliary problems 2, we are able to compute the averaged-in-time flow rates

$$\overline{Q}^X_{dis,LAD} = \frac{1}{N} \sum_{n=1}^{N} Q^X_{dis,LAD}(t^n).$$

Final problems. *Surgically-treated* geometries (one for each degree of stenosis, see Figure 1, right) with the following boundary conditions:

- Flow rate condition (18) on Γ^{in}_{LMCA};
- Flow rate condition at Γ^{in}_{LIMA}:

$$\int_{\Gamma^{in}_{LIMA}} \boldsymbol{u}^n \cdot \boldsymbol{n}\, d\gamma = Q^X_{LIMA}(t^n) \qquad X = 40, \dots, 90,$$

where

$$Q^X_{LIMA}(t^n) = \gamma^X_{LIMA} \widetilde{Q}_{LIMA}(t^n), \tag{20}$$

with

$$\gamma^X_{LIMA} = \frac{\overline{Q}^H_{LAD} - \overline{Q}^X_{dis,LAD}}{\frac{1}{N}\sum_{n=1}^{N} \widetilde{Q}_{LIMA}(t^n)}. \tag{21}$$

This choice allows us to satisfy

$$\overline{Q}^X_{LIMA} = \overline{Q}^H_{LAD} - \overline{Q}^X_{dis,LAD},$$

that is, the average in time of condition (17).

- Flow rate condition at Γ^{out}_{LAD}:

$$\int_{\Gamma^{out}_{LAD}} \boldsymbol{u}^n \cdot \boldsymbol{n}\, d\gamma = Q^X_{LAD}(t^n) \qquad X = 40, \dots, 90,$$

where Q^X_{LAD} is computed owing to (17) and remembering that $Q^X_{LAD} = Q^X_{dis,LAD}$;

- Zero-traction condition (19) at Γ^{out}_{LCx}.

In order to prescribe the flow rate conditions established above, we use the Augmented Formulation proposed in Formaggia et al [11] and Veneziani and Vergara [50]. This formulation is based on augmenting the Navier-Stokes equations with further unknowns (the Lagrange multipliers, one for each flow rate condition) and of corresponding scalar equations that implicitly enforce the flow rate conditions.

Each simulation is run for two cardiac cycles in order to eliminate transient effects, and only the data retrieved from the final cardiac cycle are used for the post-processing so as to obtain solutions independent of the initial conditions.

3 Results

For the three patients under investigation and for each degree of stenosis, we report in Figure 5, left, the flow division between LMCA and LAD, representing the ratio between LAD and LMCA flow rates computed with (9). We also report the flow division computed with the original Murray's law (equation (11)), which of course is independent of the degree of stenosis and it is constant in time since it is based on the Newtonian assumption. In particular, these values are equal to 0.6, 0.65 and 0.66 for patients P1, P2 and P3, respectively. On the right, we report the LIMA flow rate Q^X_{LIMA} computed for each degree of stenosis by means of (20)-(21). From these figures, it is clear that the original Murray's law overestimates the flow division computed with (9) in the case of a stenotic daughter vessel. As we might expect, the flow division estimated by (9) decreases for increasing degrees of LAD stenosis. Accordingly, the LIMA flow rate increases for increasing degrees of LAD stenosis, in order to maintain the distal flow rate constant.

For a more quantitative comparison between the flow division computed with the original and the extended Murray's laws, we report in Table 2, columns N-N, the time-averaged flow division between LMCA and LAD computed with (9) in the case of non-Newtonian rheology, for each patient and each degree of stenosis. For the sake of comparison, the averaging is performed starting from time instant $0.3s$ to the end of the cardiac cycle, that is, the time interval where the flow division is nearly constant. Comparing these values with the ones computed with the original Murray's law (11), we obtain percentage differences ranging in $30.2\% - 99.5\%$ for P1, $47.8\% - 99.7\%$ for P2, and $47.4\% - 99.7\%$ for P3, which confirm the increasing overestimation of the flow division computed with the original Murray's law (11) for increasing degrees of the daughter vessel stenosis.

In order to investigate also the influence of the non-Newtonian blood rheology on the proposed flow division law, we report in Table 2, columns N, the time-averaged flow division between LMCA and LAD computed with (9) for each patient and each degree of stenosis, by considering a Newtonian rheology, i.e. by assuming a constant prescribed viscosity. The percentage differences between the Newtonian and non-Newtonian flow divisions range in $9.6\% - 85\%$ for P1, $18\% - 85.7\%$ for P2, and $16.2\% - 85.7\%$ for P3. We notice that the percentage difference increases for increasing degree of stenosis, consistently with the fact that the hypothesis of Newtonian blood rheology is less and less valid for decreasing shear rates, i.e. for increasing degree of stenosis.

To better analyze the flow distribution in LIMA and LAD, in Figures 6,

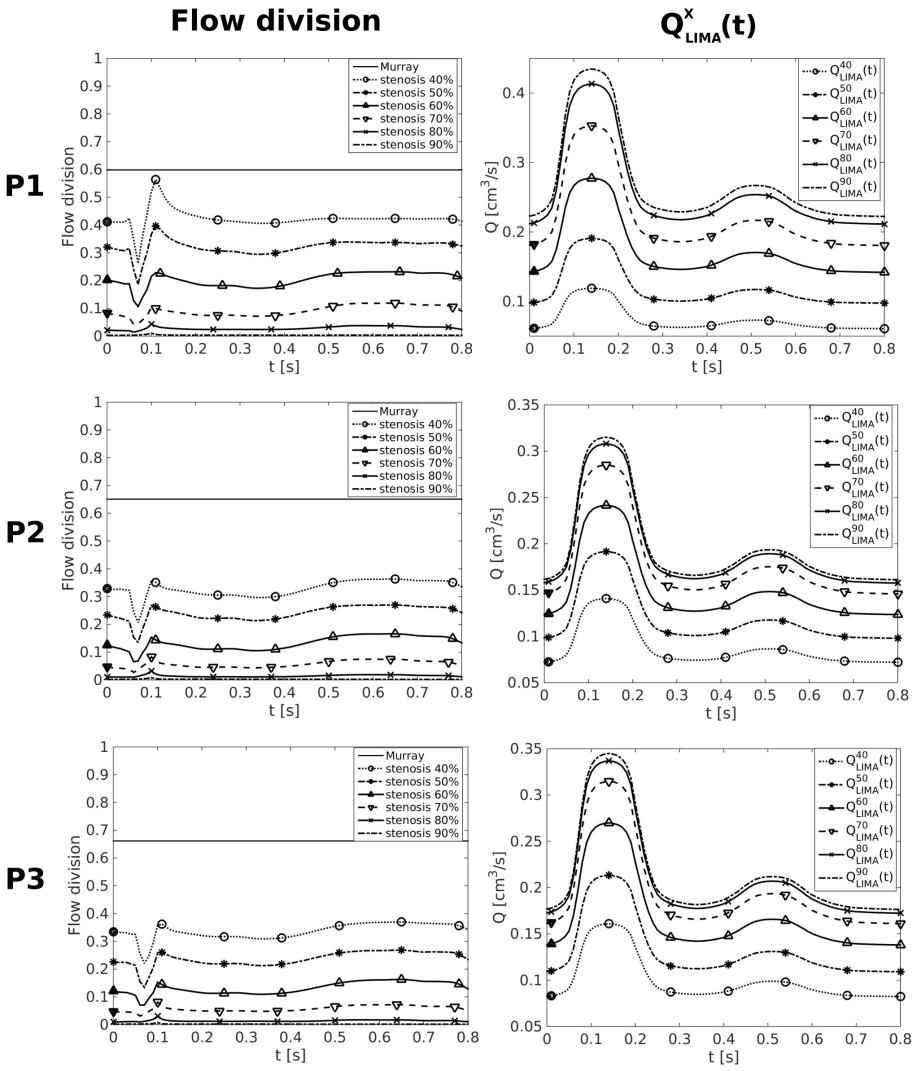

Figure 5: Left: flow division between LMCA and LAD for different degrees of stenosis computed with (9), together with the flow division computed with the original Murray's law (equation (11)). Right: LIMA flow rate Q^X_{LIMA} for each degree of stenosis

Table 2: Time-averaged flow division computed with (9) for Newtonian (N) and non-Newtonian (N-N) rheology, for each patient and for each degree of stenosis. The values of the flow division in the non-stenotic Newtonian case (Murray's law) computed with (11) are 0.6, 0.65, and 0.66 for P1, P2, and P3, respectively

	40%		50%		60%		70%		80%		90%	
	N	N-N	N	N-N	N	N-N	N	N-N	N	N-N	N	N-N
P1	0.464	0.419	0.383	0.325	0.280	0.212	0.171	0.100	0.079	0.031	0.020	0.003
P2	0.413	0.339	0.316	0.251	0.215	0.144	0.125	0.062	0.056	0.015	0.014	0.002
P3	0.414	0.347	0.315	0.248	0.214	0.142	0.124	0.062	0.056	0.015	0.014	0.002

7 and 8 we report the diastolic velocity field for P1, P2 and P3, respectively. In particular, for each degree of stenosis, we plot the velocity vectors (color-coded by the velocity magnitude) in the whole geometry, in the stenosis and in the anastomotic region. These results confirm that the flow field is greatly influenced by the degree of LAD stenosis: the higher the degree of LAD stenosis, the lower the LAD blood flow velocity (and, hence, the lower the LAD blood flow rate). On the other hand, high degrees of LAD stenosis feature higher blood flow rates in LIMA bypass in order to contrast the diminished LAD flow rate.

In order to evaluate the risk of restenosis at the anastomosis between LIMA and LAD, we report in Figure 9 the Relative Residence Time (RRT) distribution for each patient and for each degree of stenosis. RRT is a function of space defined on the lumen boundary which is known to be related to the risk of plaque formation in carotids [24] and in coronaries [22], and it is considered as a robust and single metric of low and/or oscillatory WSS. In particular, it is defined as

$$RRT(\boldsymbol{x}) = \frac{1}{(1-2OSI(\boldsymbol{x}))TAWSS(\boldsymbol{x})},$$

where OSI is the Oscillatory Shear Index

$$OSI(\boldsymbol{x}) = \frac{1}{2}\left(1 - \frac{\left\|\int_0^T \boldsymbol{\tau}_w(t,\boldsymbol{x})dt\right\|}{\int_0^T \|\boldsymbol{\tau}_w(t,\boldsymbol{x})\|\,dt}\right)$$

and $TAWSS$ is the Time-Averaged Wall Shear Stress

$$TAWSS(\boldsymbol{x}) = \frac{1}{T}\int_0^T \|\boldsymbol{\tau}_w(t,\boldsymbol{x})\|\,dt,$$

$\boldsymbol{\tau}_w = \boldsymbol{t} - (\boldsymbol{t}\cdot\boldsymbol{n})\boldsymbol{n}$ being the Wall Shear Stress vector and $\boldsymbol{t} = 2\mu\boldsymbol{D}\boldsymbol{n}$ the traction vector acting on a surface with normal $\boldsymbol{n}$. These quantities are computed in a region of interest located at the level of the anastomosis (see Figure 9), i.e. where a new plaque may in principle develop. By looking at this figure, we notice that RRT values are higher in the cases with lower degree of stenosis for all the three patients. This general trend is also confirmed by the averaged-in-space RRT values reported in Table 3. We notice that for P2 and P3 the region with high RRT values extend to all the bypass. For P1, the values far from the anastomosis are comparable to those of P2 and P3, whereas increased

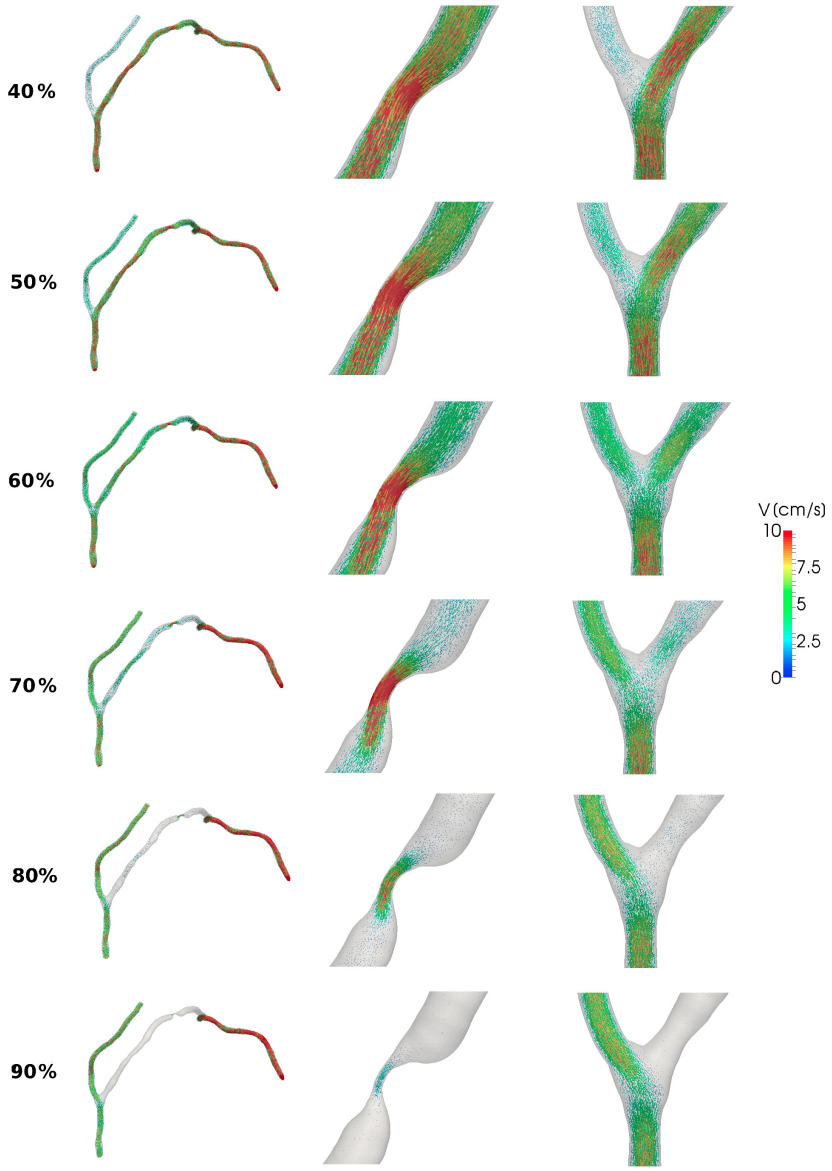

Figure 6: Velocity field at diastole, case P1. For each degree of stenosis, the velocity vectors (color-coded by velocity magnitude) in the whole geometry (left), in the stenosis (middle) and in the anastomotic region (right) are shown

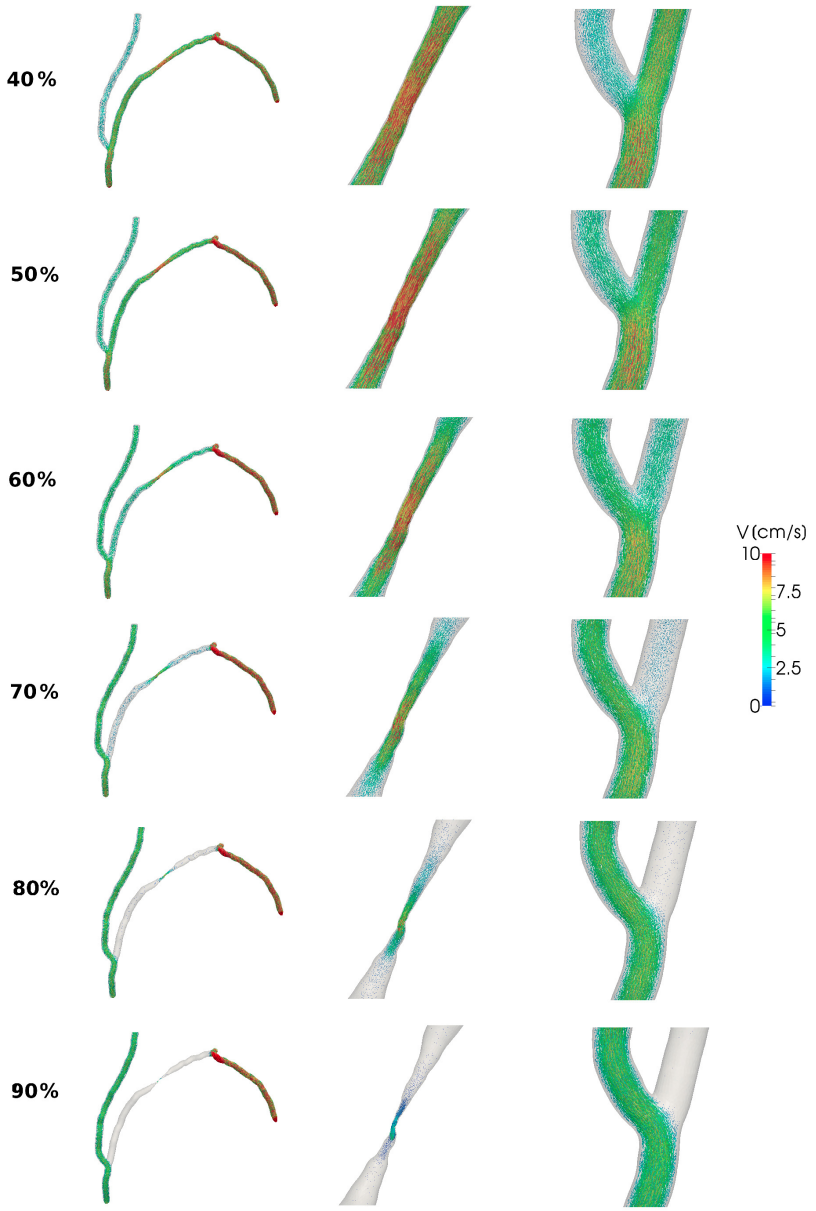

Figure 7: Velocity field at diastole, case P2. For each degree of stenosis, the velocity vectors (color-coded by velocity magnitude) in the whole geometry (left), in the stenosis (middle) and in the anastomotic region (right) are shown

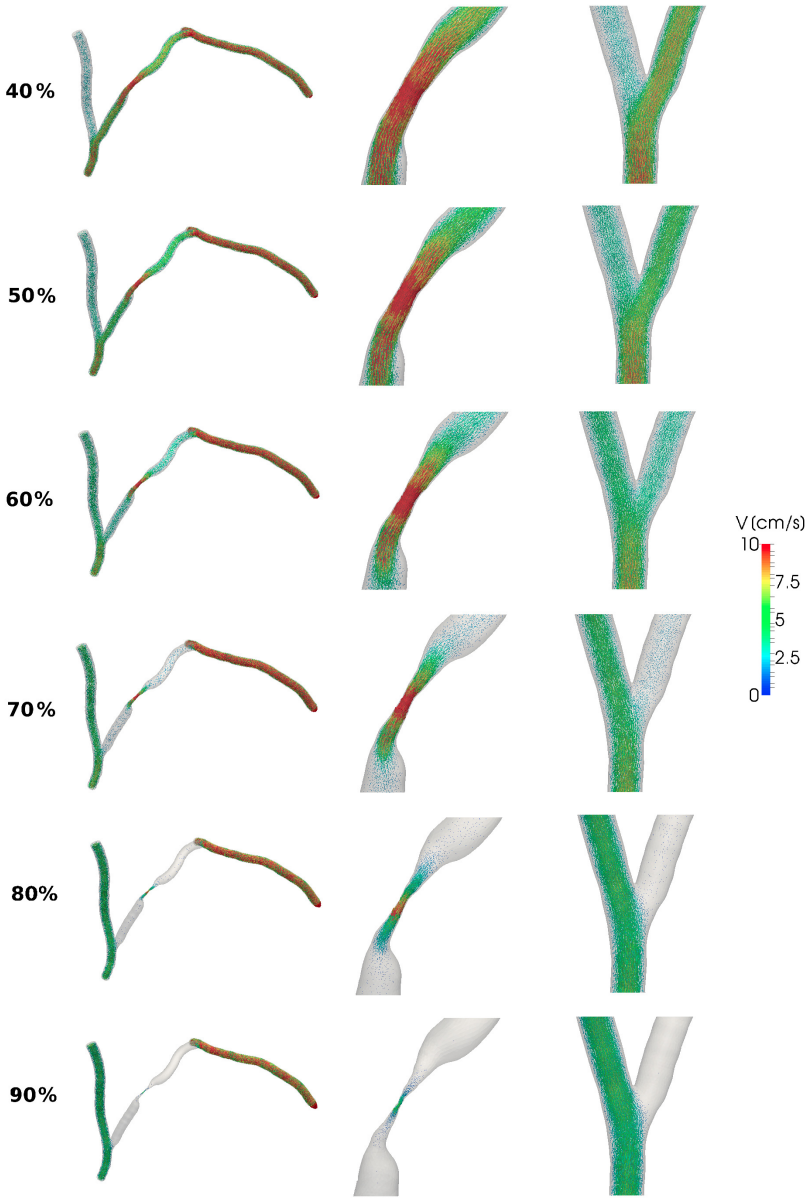

Figure 8: Velocity field at diastole, case P3. For each degree of stenosis, the velocity vectors (color-coded by velocity magnitude) in the whole geometry (left), in the stenosis (middle) and in the anastomotic region (right) are shown

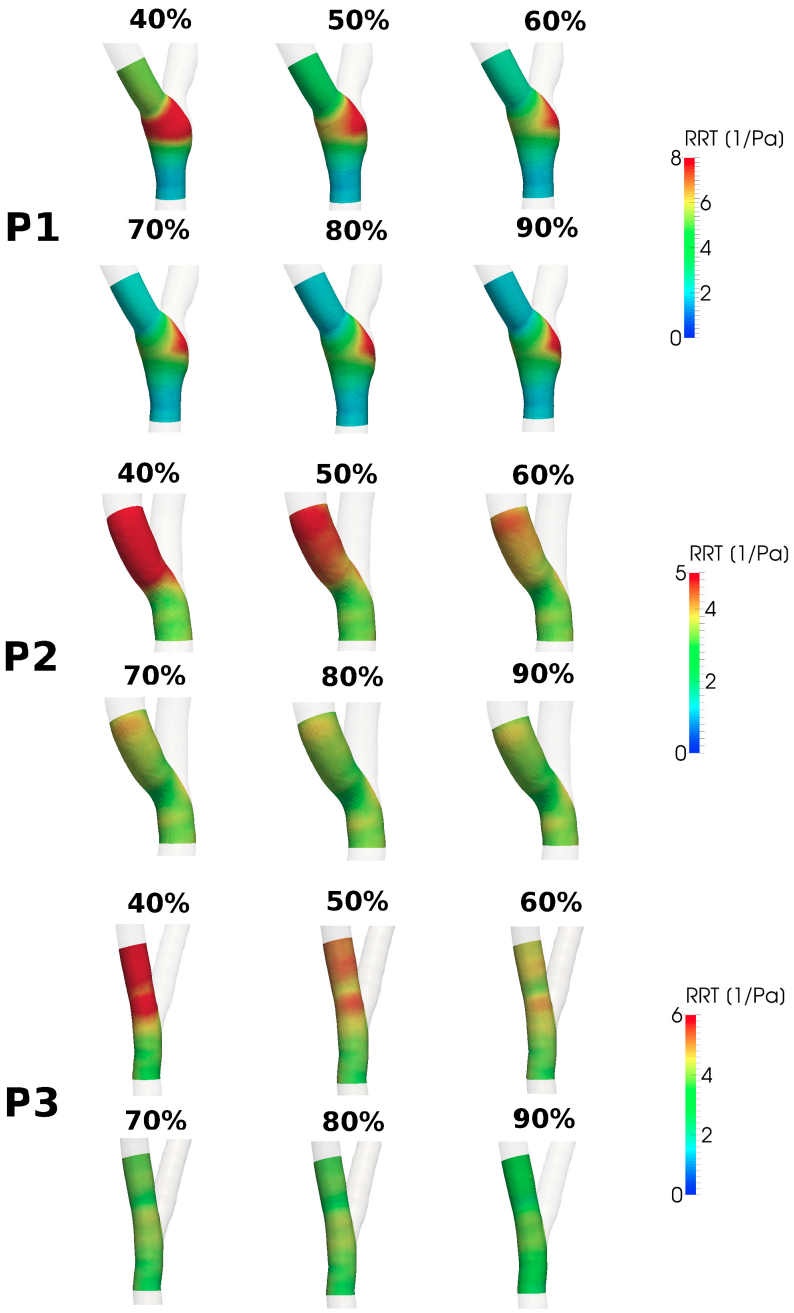

Figure 9: RRT distributions for the three patients and for each degree of stenosis

Table 3: Averaged-in-space RRT values (in Pa^{-1}) for each patient with different degrees of stenosis

	40%	50%	60%	70%	80%	90%
P1	4.65	3.77	3.28	3.13	3.07	3.05
P2	4.57	3.90	3.47	3.19	3.09	3.06
P3	4.29	3.77	3.43	3.23	3.17	3.12

Table 4: Percentage of area exposed to RRT values greater than $4Pa^{-1}$ for each patient with different degrees of stenosis

	40%	50%	60%	70%	80%	90%
P1	60.2%	29.4%	15.6%	12.9%	12.7%	12.6%
P2	59.9%	45.4%	9.5%	0.5%	0.0%	0.0%
P3	57.4%	42.9%	1.4%	0.2%	0.1%	0.0%

RRT values are observed at the anastomosis. This is probably due to the visible enlargement of the region of the anastomosis in patient P1, which may cause a more disturbed fluid dynamics, thus leading to recirculation zones and, hence, higher values of RRT.

In Table 4 we report the percentage of area of interest with RRT values greater than $4Pa^{-1}$ for each patient and for each degree of stenosis. This threshold value is chosen as a representative value to separate low and high RRT regions and is in accordance with other studies on coronaries, see e.g. Zhang et al [56]. These results clearly highlight that the regions with high RRT values become wider for decreasing degrees of stenosis, reaching values greater than 50% for all cases when the stenosis is 40%. We observe that the region of high RRT is in general more extended for patient P1, in particular for stenoses greater than 70%. Again, this is probably due to the accentuated recirculation zones caused by the enlarged anastomosis.

4 Discussion

4.1 State of the art and choice of the computational model

Many computational studies have focused their attention on blood flow characteristics at the anastomotic region of coronary bypasses, mainly in rigid domains [41, 42, 47, 55]. Regarding fluid-structure interaction (FSI) simulations in CABGs, some studies showed that the velocity patterns and qualitative distribution of WSS parameters are not significantly affected by wall compliance [19, 26]. Nevertheless, from clinical and in-vivo observations, it is known that the mismatch between the compliance of the native artery and the graft at the anastomosis can lead to graft failure [2, 46]. In particular, it is assumed that the occurrence of intimal hyperplasia around the suture line is caused by the tissue remodeling as a response to mechanical injury brought about by the artery-graft compliance mismatch. In this case, an FSI analysis is mandatory in order to describe the remodeling at the anastomotic region. However, in this

work we were interested in hemodynamic quantities, focusing on the comparisons between configurations with different degrees of stenosis, rather than on the influence of the compliance mismatch, so that we assumed rigid walls, believing that the results of these comparisons should not be influenced so much by the wall assumption.

As for blood rheology, although the assumption of Newtonian flow is generally accepted for blood flow in medium-sized arteries, as are the coronaries, some authors [8, 19, 53] demonstrated that arterial flow and WSS distribution in CABGs may be affected by the rheological properties of blood. In particular, Chen et al [8] reported significant differences in velocity profiles, secondary flow patterns and WSS distributions between the Newtonian and non-Newtonian flows, especially in the region of the graft anastomosis. For this reason, we considered a non-Newtonian model to describe blood rheology in the numerical simulations, namely the Carreau-Yasuda model, which is commonly used in hemodynamics since it is able to correctly describe the physiological shear-thinning behavior of blood (i.e. featuring decreasing viscosity for increasing shear rates) [44].

Regarding the prescription of the boundary conditions in the numerical simulations, the use of patient-specific data is a critical issue in order to obtain realistic and accurate solutions. However, clinical measurements (e.g. Doppler velocity measures or pressure measures) may be sometimes difficult to obtain, especially for deep arteries, such as the coronaries. When patient-specific data are not available, complex multiscale lumped parameters [21, 41] or impedance models [18] may for instance be used. Nevertheless, these models need a fine tuning of several parameters (e.g. resistances, conductances, inductances, impedances), which is a challenging task, especially in case of diseased vessels. For this reasons, we proposed the alternative methodology described in Section 2.4 for a realistic estimation of the flow rates to be prescribed as boundary conditions at the sections of the computational domain in absence of any clinical data. This technique is based on the computation of the flow division between LMCA and LAD arteries thanks to the proposed extended Murray's law (see below) and on the assumption that the flow rate perfusing the myocardium is independent of the presence of the LIMA bypass and the degree of LAD stenosis.

The choice of the Augmented Formulation for the prescription of the flow rate conditions allowed avoiding the introduction of any bias due to the a-priori choice of the spatial velocity profile. Indeed, this formulation was shown to be accurate to recover analytical solution and was successfully applied for clinical applications, such as for the case of aortic bicuspid valves [51, 54], abdominal aortic aneurysms [35] and carotid arteries [15].

Concerning the analysis of the association between the degree of proximal LAD stenosis and graft patency, we cite, among the computational studies, the pioneering work by Noorgard et al [32], were 3D porcine CABG models with high, partial and no competitive flows were studied; the work by Ding et al [10], who studied the impact of competitive flow on idealized LIMA-LAD models; the work by Swillens et al [48], who performed numerical simulations in geometries obtained from porcine coronaries. At the best of the authors' knowledge, the present work is the first attempt at finding, by means of computational tools, a possible relationship between different degrees of LAD stenosis and risk of LIMA restenosis in human patient-specific geometries.

4.2 On the extension of Murray's law to stenotic vessels and non-Newtonian rheology

In order to estimate the flow division between LMCA and LAD, we developed an extension of Murray's law to the case of stenotic vessels and non-Newtonian rheology, described in Section 2.3. This was necessary because in our geometries one of the daughter vessel (LAD) was stenotic. In fact, Murray's law is neither valid for stenotic vessels, as shown e.g. by Groen et al [14], nor for non-Newtonian flows [30], thus implying the need of either patient-specific data (not available in our case) or appropriate choices of outflow boundary conditions. Revellin et al [37] first generalized Murray's law to a non-Newtonian model of blood for the power-law model. Instead, the extended Murray's law here proposed can be potentially used for any non-Newtonian model. Furthermore, as far as we know, this is the first attempt at generalizing Murray's law to the stenotic case. Lindström [27] extended Murray's law to non-linear wall mechanics, an aspect we do not need to exploit here as we performed rigid-wall numerical simulations.

By inspecting Figure 5, left, we notice that the original Murray's law clearly overestimated the flow division in presence of a stenotic daughter vessel with respect to the proposed extended law. As expected, the latter was very sensible to the degree of the stenosis, providing a flow division that decreased for increasing values of the stenosis. The percentage differences between the values computed with the original and the extended Murray's laws were very relevant also in the case of 40% stenosis degree (difference greater than 47% for P2 and P3). The inappropriateness of the original Murray's law in presence of a stenosis is also highlighted by noticing that it would produce a flow rate in LAD which is independent of the degree of stenosis. Thus, this flow rate would result the same of the healthy case, i.e $Q^H_{LAD} = Q^X_{dis,LAD}$. This means that, owing to (17), we would obtain $Q^X_{LIMA} = 0$ for each X, suggesting that the use of the proposed extended Murray's law is in this case fundamental to obtain realistic boundary conditions.

In order to analyze the effects of including non-Newtonian models in the computation of the flow division, we also compared our modified Murray's law in the cases of Newtonian and non-Newtonian rheology. Looking at Table 2, it is evident that the non-Newtonian cases featured lower values of the flow division, and that the percentage difference between Newtonian and non-Newtonian models increased for increasing degrees of LAD stenosis. This is in accordance with the shear-thinning behavior of blood, taken into account by the Carreau-Yasuda model, in that higher degrees of stenosis feature higher resistances to blood flow, hence resulting in decreased flow divisions and lower shear rates and, eventually, higher blood viscosity. Based on our results, we can claim that not only is the use of a non-Newtonian model important in order to obtain more realistic solutions in the numerical simulations themselves, as already discovered e.g. by Chen at al [8], but it is also important when estimating the flow division in a bifurcation and, hence, when estimating the flow rates to be prescribed in the numerical simulations.

4.3 On the influence of LAD stenosis on the risk of anastomotic restenosis

According to Berger et al [4], the degree of stenosis is one of the most important factor affecting the incidence of LIMA graft occlusion. In particular, they reported an incidence of LIMA graft occlusion up to 79% when the native coronary stenosis is less than 50%. Although the aetiology of graft failure due to competitive flow has not been thoroughly investigated, most clinical studies on graft patency and competitive flow show a better long-term patency of grafts when coronaries with severe stenosis are bypassed, compared with grafts placed distal to non-significant stenosis [4, 5, 52]. Meng et al [29] studied the influence of competitive flow on LIMA graft flow using a swine model by varying the degree of stenosis in the proximal LAD with a flow occluder. They observed that the higher the degree of stenosis in the proximal LAD, the lower the competitive flow in LAD and the higher the mean flow in LIMA. The same trend is also confirmed, for instance, in the works by Pagni et al [33, 34]. Similar results were also reported in Noorgard et al [31], who measured transit-time flow patterns at four different flow conditions in a LIMA-to-LAD bypass of a porcine model and concluded that the LIMA graft is much influenced by competitive flow, as both full and partial competitive flow conditions significantly altered the flow patterns.

Looking at Figures 6, 7 and 8, we observe that our results are in accordance with these findings. In particular, the degree of LAD stenosis greatly influenced the flow pattern at the anastomosis, as low degrees of stenosis resulted in high competitive flow between LIMA and LAD. Consequently, competitive flow may cause particularly "disturbed" flow at the region of the anastomosis, possibly resulting in recirculation and stagnation zones. Such flow features typically correspond to low and oscillating WSS and long particle residence times, which are the main hemodynamic features that have been correlated with atherogenesis and intimal hyperplasia [25, 28]. Indeed, as we can see from Figure 9 and Tables 3 and 4, higher competitive flows due to lower degrees of LAD stenosis resulted in higher values of RRT at the anastomosis and in the LIMA graft. According to Caro's "shear-dependent mass transfer" theory [6], these high RRT values may influence the endothelial function allowing for an increase of the permeability to lipo-proteins, resulting in intimal thickening and hence causing LIMA graft failure.

Besides the possible risk of restenosis at the anastomosis site, some authors have also noted a possible diffuse narrowing of LIMA grafts along its whole length, the so-called "string-phenomenon" [1, 52]. This is particularly evident in patients with less-than-critical stenosis of the recipient artery, suggesting that competitive flow may cause the string phenomenon and subsequent graft failure [57]. Looking at Figure 9, we notice that the regions of high RRT values extended in fact also to the LIMA bypass. This is particularly evident for patients P2 and P3, but we can still appreciate higher and higher RRT values for increasing degrees of stenosis in the LIMA bypass of patient P1. These high values of RRT may explain the string phenomenon occurring in the LIMA bypass when the LAD stenosis is not critical. In particular, high competitive flow due to the presence of a non-critical stenosis, which means lower and disturbed graft flow characterized by low and oscillatory WSS, may induce the LIMA graft to narrow its lumen in order to maintain WSS within certain limits.

5 Conclusions and limitations

The purpose of this study was to investigate the effects of competitive flow on the hemodynamics in LIMA-to-LAD bypass grafts. In particular, we considered three patients in which the degree of LAD stenosis was virtually varied in order to produce different degrees of competitive flow. For the prescription of the boundary conditions in the numerical simulations, and in particular to compute the flow division between LMCA and LAD, we proposed an extension of Murray's law to stenotic vessels and non-Newtonian rheology. The main results of our numerical investigation can be summarised as follows:

1. The original Murray's law overestimates the flow division when one of the daughter vessels is stenotic, whereas the proposed extended Murray's law is able to correctly detect different degrees of LAD stenosis, providing decreasing values of the flow rate in the daughter vessel for increasing values of the stenosis;

2. When using the extended Murray's law, the non-Newtonian rheology of blood should be taken into account, since the differences in the computation of the flow division using the (less-realistic) Newtonian and the non-Newtonian models are significant, even for low degrees of the daughter vessel stenosis;

3. Lower degrees of LAD stenosis cause higher competitive flow between LIMA and LAD, possibly resulting in disturbed flow at the anastomosis;

4. Disturbed flow at the anastomosis causes recirculation and stagnation zones with low and oscillating WSS and, hence, high RRT values. As a result, endothelial function and mass transport may be influenced, hence possibly leading to intimal thickening and subsequent graft failure.

The proposed extended Murray's law used in combination with the methodology developed for the estimation of the flow rates, may be a suitable alternative to the prescription of realistic boundary conditions in the numerical simulations when such data are unavailable.

From a clinical perspective, these results confirm the evidence that the long-term patency of LIMA graft may be greatly affected by the stenosis degree of the native LAD, as low degrees of LAD stenosis may result in higher hemodynamic indices related to the risk of restenosis in the anastomosis.

A potential limitation of this study is the assumption of rigid walls. However, as already pointed out in the Discussion (Section 4.1), we do not expect the dynamics of the vessel walls to substantially affect the results of our comparison. Analyzing the effects of compliance mismatch between LIMA and LAD on the risk of anastomotic restenosis is nonetheless worth being investigated. Secondly, a clinical validation of the proposed extended Murray's law is needed to understand its real applicability. Fluid-structure interaction and clinical experiments for the validation of the extended Murray's law will be the focus of our future works.

Acknolwdgements

CV and AQ have been partially supported by the Italian MIUR PRIN09 project no. 2009Y4RC3B 001.

References

[1] H. B. Barner. Double internal mammary-coronary artery bypass. *Arch. Surg.*, 109:627–630, 1974.

[2] H. S. Bassiouny, S. White, S. Glagov, E. Choi, D. P. Giddens, and C. K. Zarins. Anastomotic intimal hyperplasia: mechanical injury or flow induced. *J. Vasc. Surg.*, 15:708–717, 1992.

[3] J. F. Beltrame, R. Dreyer, and R. S. Tavella. *Coronary Artery Disease - Current Concepts in Epidemiology, Pathophysiology, Diagnostics and Treatment*. InTech, 2012.

[4] A. Berger, P. A. MacCarthy, U. Siebert, S. Carlier, W. Wijns, G. Heyndrickx, J. Bartunek, H. Vanermen, and B. D. Bruyne. Long-term patency of internal mammary artery bypass grafts - Relationship with preoperative severity of the native coronary artery stenosis. *Circulation*, 110:36–40, 2004.

[5] C. G. Botman, J. Schonberger, S. Koolen, O. Penn, H. Botman, N. Dib, E. Eeckhout, and N. Pijls. Does stenosis severity of native vessels influence bypass and graft patency? A prospective fractional flow reserve-guided study. *Ann. Thorac. Surg.*, 83:2093–2097, 2007.

[6] C. G. Caro, J. M. Fitz-Gerald, and R. C. Schroter. Atheroma and arterial wall shear. Observation, correlation and proposal of a shear dependent mass transfer mechanism for atherogenesis. *Proc. R. Socc London, Ser. B*, 117:109–159, 1971.

[7] Y. A. Cengel and J. M. Cimbala. *Fluid Mechanics - Fundamentals and Applictions*. McGraw-Hill, 2006.

[8] J. Chen, X.-Y. Lu, and W. Wang. Non-newtonian effects of blood flow on hemodynamics in distal vascular graft anastomoses. *J. Biomech.*, 39:1983–1995, 2006.

[9] Y. I. Cho and K. R. Kensey. Effects of the non-Newtonian viscosity of blood on flows in a diseased arterial vessel. *Biorheology*, 28:241–262, 1991.

[10] J. Ding, Y. Liu, F. Wang, and F. Bai. Impact of competitive flow on hemodynamics in coronary surgery: numerical study of ITA-LAD model. *Computat. Math. Methods Med.*, 2012, 2012. doi:10.1155/2012/356187.

[11] L. Formaggia, J. F. Gerbeau, F. Nobile, and A. Quarteroni. Numerical treatment of defective boundary conditions for the Navier-Stokes equation. *SIAM J. Numer. Anal.*, 40(1):376–401, 2002.

[12] L. Formaggia, A. Quarteroni, and A. Veneziani. *Cardiovascular Mathematics: Modeling and Simulation of the Circulatory System, Modeling, Simulation and Application.* Springer, 2009.

[13] M. H. Friedman, C. B. Bargeron, O. J. Deters, G. M. Hutchins, and F. F. Mark. Correlation between wall shear and intimal thickness at a coronary artery branch. *Atherosclerosis*, 68:27–33, 1987.

[14] H. C. Groen, L. Simons, Q. J. van den Bouwhuijen, Q. J. Bosboom, F. J. Gijsen, A. G. van der Giessen, F. N. van de Vosse, A. Hofman, A. F. van der Steen, J. C. Wittemann, A. van der Lugtm, and J. J. Wentzel. MRI-based quantification of outflow boundary conditions for computational fluid dynamics of stenosed human carotid arteries. *J. Biomech.*, 43(12):2332–2338, 2010.

[15] B. Guerciotti, C. Vergara, L. Azzimonti, L. Forzenigo, A. Buora, P. Biondetti, and M. Domanin. Computational study of the fluid-dynamics in carotis before and after endarterectomy. *J. Biomech.*, 49:26–38, 2016.

[16] L. D. Hillis, P. K. Smith, J. L. Anderson, J. A. Bittl, C. R. Bridges, J. G. Byrne, J. E. Cigarroa, V. J. DiSesa, L. F. Hiratzka, A. M. Hutter, M. E. Jessen, E. C. Keeley, S. J. Lahey, R. A. Lange, M. J. London, M. J. Mack, M. R. Patel, J. D. Puskas, J. F. Sabik, O. Selnes, D. M. Shahian, J. C. Trost, and M. D. Winniford. ACCF/AHA guideline for coronary artery bypass graft surgery. *Circulation*, 124:652–735, 2011.

[17] M. Hofer, G. Rappitsch, K. Perktold, W. Trubel, and H. Schima. Numerical study of wall mechanics and fluid dynamics in end-to-side anastomoses and correlation to intimal hyperplasia. *J. Biomech.*, 29:1297–1308, 1996.

[18] D. A. Johnson, U. P. Naik, and A. N. Beris. Efficient implementation of the proper outlet flow conditions in blood flow simulations through asymmetric arterial bifurcations. *Int. J. Numer. Meth. Fluids*, 66:1383–1408, 2011.

[19] F. Kabinejadian and D. N. Ghista. Compliant model of a coupled sequential coronary arterial bypass graft: effects of vessel wall elasticity and non-newtonian rheology on blood flow regime and hemodynamic parameters distribution. *Med. Eng. Phys.*, 34:860–872, 2012.

[20] J. Keegan, P. D. Gatehouse, G. Z. Yang, and D. N. Firmin. Spiral phase velocity mapping of left and right coronary artery blood flow: correction for through-plane motion using selective fat-only excitation. *J. Magn. Reson. Im.*, 20:953–960, 2004.

[21] H. J. Kim, I. E. Vignon-Clementel, C. A. Figueroa, K. E. Jansen, and C. A. Talor. Developing computational methods for three-dimensional finite element simulations of coronary blood flow. *Finite Elem. Anal. Des.*, 46:514–525, 2010.

[22] J. Knight, U. Olgac, S. C. Saur, D. Poulikakos, W. J. Marshall, P. C. Cattin, H. Alkadhi, and V. Kurtcuoglu. Choosing the optimal wall shear parameter for the prediction of plaque location - A patient-specific computational study in human right coronary arteries. *Atherosclerosis*, 211(2):445–450, 2010.

[23] E. Kouhi, Y. S. Morsi, and S. H. Masood. Haemodynamic analysis of coronary artery bypass grafting in a non-linear deformable artery and newtonian pulsatile blood flow. *Proc. Inst. Mech. Eng. H.*, 222(8):1273–1287, 2008.

[24] S. W. Lee, L. Antiga, and D. A. Steinman. Correlations among indicators of disturbed flow at the normal carotid bifurcation. *J. Biomech. Eng.*, 131(6):061013, 2009. doi:10.1115/1.3127252.

[25] M. S. Lemson, J. H. M. Tordoir, M. J. A. P. Daemen, and P. J. E. H. M. Kitslaar. Intimal hyperplasia in vascular grafts. *Eur. J. Vasc. Endovasc. Surg.*, 19:336–350, 2000.

[26] A. Leuprecht, K. Perktold, M. Prosi, T. Berk, W. Trubel, and H. Schima. Numerical study of hemodynamics and wall mechanics in distal end-to-side anastomoses of bypass grafts. *J. Biomech.*, 35:225–236, 2002.

[27] S. B. Lindström, G. Satha, and A. Klarbring. Extension of Murray's law including nonlinear mechanics of a composite artery wall. *Biomech Model Mechanobiol*, 14:83–91, 2015.

[28] F. Loth, P. F. Fischer, and H. S. Bassiouny. Blood flow in end-to-side anastomoses. *Annu. Rev. Fluid. Mech.*, 40:367–393, 2008.

[29] X. Meng, Q. Fu, W. Sun, J. Yu, Y. W, and W. Bi. Competitive flow arising from varying degrees of coronary artery stenossi affects the blood flow and the production of nitric oxide and endothelin in the internal mammary artery. *Eur. J. Cardio-Thorac.*, 43:1022–1027, 2013.

[30] C. D. Murray. The physiological principle of minimum work. the vascular system and the cost of blood volume. *Proc. Natl. Acad. Sci.*, 12:207–214, 1926.

[31] H. Nordgaard, D. Nordhaug, I. Kirkeby-Garstad, L. Lovstakken, N. Vitale, and R. Haaverstad. Different graft flow patterns due to competitive flow or stenosis in the coronary anastomosis assessed by transit-time flowmetry in a porcine model. *Eur. J. Cardio-Thorac.*, 36:137–142, 2009.

[32] H. Nordgaard, A. Swillens, D. Nordhaug, I. Kirkeby-Garstad, D. Van Loo, N. Vitale, P. Segers, R. Haaverstad, and L. Lovstakken. Impact of competitive flow on wall shear stress in coronary surgery: computational fluid dynamics of a LIMA-LAD model. *Cardiovasc. Res.*, 88:512–519, 2010.

[33] S. Pagni, J. Storey, J. Ballen, W. Montgomery, B. Y. Chiang, S. Etoch, and P. A. Spence. ITA versus SVG: a comparison of instantaneous pressure and flow dynamics during competitive flow. *Eur. J. Cardio-Thorac.*, 11:1086–1092, 1997.

[34] S. Pagni, J. Storey, J. Ballen, W. Montgomery, N. K. Qaqish, S. Etoch, and P. A. Spence. Factors affecting internal mammary artery graft survival: how is competitive flow from a patent native coronary vessel a risk factor? *J. Surg. Res.*, 71:172–178, 1997.

[35] M. Piccinelli, C. Vergara, L. Antiga, L. Forzenigo, P. Biondetti, and M. Domanin. Impact of hemodynamics on lumen bounday displacements in abdominal aortic aneurysms by means of dynamic computed tomography and computational fluid dynamics. *Biomech. Model. Mechan.*, 12(6):1263–1276, 2013.

[36] A. Quarteroni. *Numerical models for differential problems*. Springer, 2009.

[37] R. Revellin, F. Rousset, D. Baud, and J. Bonjour. Extension of Murray's law using a non-newtonian modelof blood flow. *Theor Biol Med Model*, 6(7):2439–2445, 2009. doi:10.1186/1742-4682-6-7.

[38] C. S. Rihal, D. L. Raco, B. J. Gersh, and S. Yusuf. Indications for coronary artery bypass surgery and percutaneous coronary intervention in chronic stable angina: review of the evidence and methodological considerations. *Circulation*, 108:2439–2445, 2003.

[39] J. F. Sabik, B. W. Lytle, E. H. Blackstone, M. Khan, P. L. Houghtaling, and D. M. Cosgrove. Does competitive flow reduce internal thoracic artery graft patency? *Ann. Thorac. Surg.*, 76:1490–1497, 2003.

[40] H. Sakuma, S. Globits, M. O'Sullivan, A. Shimakawa, M. A. Berstein, T. K. F. Foo, T. M. Amidon, K. Takeda, T. Nakagawa, and C. B. Higgins. Breath-hold MR measurements of blood flow velocity in internal mammary arteries and coronary artery bypass grafts. *J. Magn. Reson. Im.*, 1:219–222, 1996.

[41] S. Sankaran, M. E. Moghadam, A. M. Kahn, E. E. Tseng, J. M. Guccione, and A. L. Marsden. Patient-specific multiscale modeling of blood flow for coronary artery bypass graft surgery. *Ann. Biomed. Eng.*, 40(10):2228–2242, 2012.

[42] M. Sankaranarayanan, D. N. Ghista, L. P. Chua, Y. S. Tan, and G. S. Kassab. Analysis of blood flow in an out-of-plane CABG model. *Am. J. Physiol. Heart Circ. Physiol.*, 291:H283–H295, 2242, 2006.

[43] T. F. Sherman. On connecting large vessels to smalls - The meaning of Murray's law. *J. Gen. Physiol.*, 78:431–453, 1981.

[44] S. S. Shibeshi and W. E. Collins. The rheology of blood flow in a branched arterial system. *Appl Rheo*, 15(6):398–405, 2005.

[45] R. N. Singh and J. A. Sosa. Internal mammary artery: a "live"' conduit for coronary bypass. *J. Thorac. Cardiovasc. Surg.*, 87(6):936–938, 1984.

[46] V. S. Sottiurai, J. S. T. Yao, R. C. Batson, S. L. Sue, R. Jones, and Y. A. Nakamura. Distal anastomotic intimal hyperplasia: histopathologic character and biogenesis. *Ann. Vasc. Surg.*, 3:26–33, 1989.

[47] D. A. Steinman, B. Vinh, C. R. Ethier, M. Ojha, R. S. C. Cobbold, and K. W. Johnston. A numerical simulation of flow in a two-dimensional end-to-side anastomosis model. *J. Biomech. Eng.*, 115:112–118, 1993.

[48] A. Swillens, M. De Witte, H. Nordgaard, L. Løvstakken, D. Van Loo, B. Trachet, J. Vierendeels, and P. Segers. Effect of the degree of LAD stenosis on "competitive flow" and flow field characteristics in LIMA-to-LAD bypass surgery. *Med. Biol. Eng. Comput.*, 50:839–849, 2012.

[49] J. Tatoulis, B. F. Buxton, and J. A. Fuller. Patencies of 2127 arterial to coronary conduits over 15 years. *Ann. Thorac. Surg.*, 77(1):93–101, 2004.

[50] A. Veneziani and C. Vergara. Flow rate defective boundary conditions in haemodynamics simulations. *Int. J. Numer. Meth. Fl.*, 47:803–816, 2005.

[51] C. Vergara, F. Viscardi, L. Antiga, and G. B. Luciani. Influence of bicuspid valve geometry on ascending aortic fluid-dynamics: a parametric study. *Artif. Organs*, 36(4):368–378, 2012.

[52] R. P. Villareal and V. S. Mathur. The string phenomenon - An important cause of internal mammary artery graft failure. *Tex Heart Inst. J.*, 27:346–349, 2000.

[53] J. Vimmr, A. Jonašóvá, and O. Bublík. Numerical analysis of non-Newtonian blood flow and wall shear stress in realistic single, double and triple aorto-coronary bypasses. *Int. J. Numer. Method Biomed. Eng.*, 29:1057–1081, 2013.

[54] F. Viscardi, C. Vergara, L. Antiga, S. Merelli, A. Veneziani, G. Puppini, E. Faggiano, A. Mazzucco, and G. B. Luciani. Comparative finite-element model analysis of ascending aortic flow in bicuspod and tricuspid aortic valve. *Artif. Organs*, 34(12):1114–1120, 2010.

[55] J. M. Zhang, L. P. Chua, D. N. Ghista, S. C. M. Yu, and Y. S. Tan. Numerical investigation and identification of susceptible sites of atherosclerotic lesion formation in a complete coronary artery bypass model. *Med. Biol. Eng. Comput.*, 46(7):689–699, 2008.

[56] J. M. Zhang, T. Luo, S. Y. Tan, A. M. Lomarda, A. S. Wong, F. Y. Keng, J. C. Allen, Y. Huo, B. Su, X. Zhao, M. Wan, G. S. Kassab, R. S. Tan, and L. Zhong. Hemodynamic analysis of patient-specific coronary artery tree. *Int. J. Numer. Method Biomed. Eng.*, 1(4):e02708, 2015.

[57] X. Zhao, Y. Liu, L. Li, W. Wang, J. Xie, and Z. Zhao. Hemodynamics of the string phenomenon in the internal thoracic artery grafted to the left anterior descending artery with moderate stenosis. *J. Biomech.*, 2015. doi:10.1016/j.jbiomech.2015.11.044.

MOX Technical Reports, last issues

Dipartimento di Matematica
Politecnico di Milano, Via Bonardi 9 - 20133 Milano (Italy)

12/2016 Bartezzaghi, A.; Dedè, L.; Quarteroni, A.
Isogeometric Analysis of Geometric Partial Differential Equations

11/2016 Zhu, S.; Dedè, L.; Quarteroni, A.
Isogeometric Analysis and proper orthogonal decomposition for the acoustic wave equation

10/2016 Flemisch, B.; Fumagalli, A.; Scotti, A.
A review of the XFEM-based approximation of flow in fractured porous media

08/2016 Dassi, F.; Perotto, S.; Si, H.; Streckenbach, T.
A priori anisotropic mesh adaptation driven by a higher dimensional embedding

09/2016 Rizzo, C.B.; de Barros, F.P.J.; Perotto, S.; Oldani, L.; Guadagnini, A.
Relative impact of advective and dispersive processes on the efficiency of POD-based model reduction for solute transport in porous media

07/2016 Pacciarini, P.; Gervasio, P.; Quarteroni, A.
Spectral Based Discontinuous Galerkin Reduced Basis Element Method for Parametrized Stokes Problems

06/2016 Micheletti, S.; Perotto, S.; Signorini, M.
Anisotropic mesh adaptation for the generalized Ambrosio-Tortorelli functional with application to brittle fracture

05/2016 Alfio Quarteroni, A.; Lassila, T.; Rossi, S.; Ruiz-Baier, R.
Integrated Heart - Coupling multiscale and multiphysics models for the simulation of the cardiac function

01/2016 Domanin, M.; Buora, A.; Scardulla, F.; Guerciotti, B.; Forzenigo, L.; Biondetti, P.; Vergara, C.
Computational fluid-dynamic analysis of carotid bifurcations after endarterectomy: closure with patch graft versus direct suture

02/2016 Crivellaro, A.; Perotto, S.; Zonca, S.
Reconstruction of 3D scattered data via radial basis functions by efficient and robust techniques